

# An accurate power control strategy for electromagnetic rotary power controllers

Xiangwu Yan<sup>1</sup>, Chen Shao<sup>1\*</sup>, Jiaoxin Jia<sup>1</sup>, Waseem Aslam<sup>2</sup>, Weifeng Peng<sup>1</sup>, Ruoqia Yang<sup>1</sup>,

1 Key Laboratory of Distributed Energy Storage and Micro-grid of Hebei Province, North China Electric Power University Baoding 071003 China

2 Department of Electrical Engineering, University of Sargodha Sargodha 40100 Pakistan

\*shaochen@ncepu.edu.cn

**Abstract:** With the rapid development of active distribution networks, the “petal”-type distribution network has become the mainstream power supply structure. To ensure the safe and reliable power supply of a distribution system, power control methods for active distribution networks should be further studied. An electromagnetic rotary power flow controller (RPFC) is a feasible solution for active distribution network power control. However, when testing the effectiveness of the PQ decoupled control method for RPFC based on instantaneous reactive power theory, difficulties were encountered with the synchronous control of the rotor position angle of two rotating-phase transformers, and the accuracy of power control was unsatisfactory. Given this condition, PQ control is improved in three ways. First, the system periodic oscillation problem is solved via variable speed control. Second, the servo motor–rotary phase-shifting transformer synchronous rotation scheme is designed, reducing power control error and improving stability. The overshoot phenomenon in power control is improved using the variable domain fuzzy proportional–integral adaptive method. Experimental results show that the proposed advanced control scheme exhibits good dynamic and static performance in power control scenarios and achieves effective improvement of RPFC.

**Keywords:** Active distribution network; electromagnetic rotary power flow controller; power precision control; dual RPST speed-coordinated control; variable domain fuzzy PI control

## 1. Introduction

The contact line of a “petal” distribution network starts from the substation and passes through a number of switching stations to form a distribution network similar to the shape of a flower petal; in normal operation mode, power is supplied by multiple sources in combined ring operation mode [1], evidently improving the reliability of the power supply compared with a radiation-type distribution network. However, given the unsynchronized line construction and load development, a “petal”-type distribution network exhibits the characteristics of uncontrollable power size and direction [2]. Therefore, an active alternating current (AC) interconnection device is urgently required to control power effectively at the loop closure point and ensure the safe operation of the loop closure, significantly improving the power supply

reliability of a distribution network [3].

Current equipment with line power regulation capabilities include the smart soft open point (SOP) [4], the unified power flow controller (UPFC) [5], and the electromagnetic rotary power flow controller (RPFC) [6]. SOP is typically implemented as a back-to-back voltage–source converter; it provides independent control of output voltage amplitude and phase at an access point by applying a control strategy to both converters to achieve bidirectional decoupling control of active and reactive power flowing through the interconnected line [7]. UPFC dynamically regulates the active and reactive power of a line by controlling the series voltage source converter to change the voltage injected into the line by a series transformer [8]. However, SOP and UPFC are mostly based on fully controlled power electronic transformers; they have high investment and operation

---

and maintenance costs, and they cannot be used on large-scale distribution networks in the short term [9]. RPFC consists of two sets of rotary phase-shifting transformers (RPSTs) connected in series [10]. The compensating voltage of the series entry line can be flexibly controlled by changing the relative angles of the two sets of RPSTs, providing a new method for the power regulation of a power system. A comprehensive comparison of the technical characteristics of RPFC and UPFC has been conducted in the literature [11], demonstrating that RPFC can accurately control the power of a system within a response time of a 100 ms. Moreover, its cost is low, its control is relatively simple, and it exhibits good control characteristics, presenting some application prospects in the power control conditions of a distribution network. However, RPFC is still in the prototype development stage, and some control technical problems must still be solved and experimentally verified before large-scale application.

Further research on RPFC is minimal, both in China and other countries, particularly in terms of control. An RPFC power inner-loop decoupling control method that is applicable to distribution networks is not yet available. Considering that RPFC and UPFC realize line power regulation through series voltage sources and more research is available on the steady-state modeling and control strategy direction of UPFC [12], the power control strategy of UPFC can be used as reference. Existing UPFC power control methods include phase angle control [13] and vector control [14]. Phase angle control regulates line reactive power by changing the amplitude of output voltage and active power by changing the phase angle. The literature [15] established a steady-state mathematical model of RPFC and adopted the power regulation method of phase angle control to achieve effective power regulation at the receiving end of a transmission system. However, when this control strategy was applied to a distribution network, the failure of the power decoupling regulation is caused by the non-negligible line resistance. Vector control consists of a power outer loop and a current inner loop. First, the line current is decomposed into  $dq$ -axis components. Active power is considered related only to the  $q$ -axis components, while reactive power is related only to the  $d$ -axis components. The

amplitude and phase of the AC-measured voltage are calculated, and then the phase-locked loop provides the angle to transform the voltage from the  $dq$ -axis coordinates back into the abc coordinate system, and finally, the required series voltage is obtained. The literature [16] studied the UPFC power control strategy based on vector control. It compared cross-coupling control with cross-decoupling control. The former has a simpler structure, is easier to implement, and exhibits better robustness. The latter has the advantage of regulating tide quickly and decoupling completely. To address the drawbacks resulting from the poor robustness of cross-coupled control, the literature [17] proposed adding fuzzy control theory to the series-side controller to effectively improve power control challenges. Through simulation, the authors verified that an improved fuzzy proportional–integral (PI) control can considerably increase the steady-state power tracking control capability of UPFC. Therefore, RPFC power link control can be achieved by adopting a crossover decoupling control method based on instantaneous reactive power theory and improving the PI controller by using the fuzzy control method to increase the robustness of RPFC power control.

The outermost phase angle control link of RPFC has its own special working principle, and it can no longer be borrowed from UPFC. RPFC uses servo motors to control the phase angle of dual rotors, and the challenge is coordinating the control of dual servo motors. Existing dual-motor drives have two types [18]: those with independent speed rings (dual-loop) and those with a single speed ring (single-loop). As shown in the structure wherein dual RPSTs rotate independently, and thus, achieve a cascade of compensating voltages, the use of a dual-loop control structure can achieve more flexible power control effects. For the specific controller design of the dual-loop structure, existing synchronous linkage control methods include differential current negative feedback [19] and differential speed feedback [20]. The parameters of the two motors cannot be identical, even if the currents are identical. Consequently, the same control speed may not be achieved, and the use of differential speed negative feedback control is more suitable for RPFC control systems. However, the existing motor differential negative feedback control is generally fixed

speed control. One experiment found that the two-loop fixed speed RPFC control scheme exhibited poor stability under complex power control conditions; thus, it must be further improved. The literature [21] proposed a single closed-loop speed regulation method with negative feedback for variable speed motors. By collecting current speed as feedback quantity and comparing it with a given dynamic speed and then controlling the duty cycle of the output pulse-width modulation (PWM) to adjust output voltage and achieve the speed control requirement, the method achieves good response speed in the constant torque variable speed simulation. Variable speed control is an effective solution for the coordinated control of twin servo motors. Meanwhile, the influence of drive mechanism errors on the precise control of power must still be considered when moving away from the coordinated control of twin servo motors toward the realization of twin rotor phase angle control.

The RPFC power decoupling control method based on instantaneous reactive power theory is studied on the basis of the preceding research. For RPFC regulation characteristics, the speed coordination control of dual RPSTs is realized through the variable speed control scheme, which solves the periodic oscillation problem encountered by RPFC operation. Considering the shortage of the RPFC mechanical structure, the servo motor–RPFC coordinated rotation control link is designed. This link reduces the steady-state error of the system and improves the overshoot phenomenon in RPFC power control through a variable domain fuzzy PI control. Finally, a 380 V/40 kVA prototype is developed, and the experimental results show that RPFC exhibits accurate power control under various experimental scenarios, verifying the correctness of the proposed control strategy.

## 2. Construction of a power decoupling control model based on RPFC

### 2.1. Topology of RPFC

The topology of RPFC is shown in Figure 1. The rotor winding must wind a large number of coils, and thus, its mass is considerably larger than stator winding. Accordingly, the rotor side is connected in parallel to the supply line, because the primary side of the transformer and the stator side are connected to the supply line in

series as the secondary side of the transformer. Two groups of RPSTs are driven by the servo motor to synthesize two stator voltage phases of constant amplitude and the continuously adjustable phase angle. At which point, the two groups of stator voltage phases are superimposed to achieve the injection of a series voltage of adjustable amplitude and phase angle into the line.

RPST is similar to a transformer at rest, with a certain ratio between the voltage on the stator and rotor sides. Meanwhile, the phase difference is related to angles  $\alpha_1$  and  $\alpha_2$  between the stator and the rotor. For a multi-pole RPST, the rotor angle is only required to move by a small mechanical angle to change the phase amount of voltage strung into the line [6].

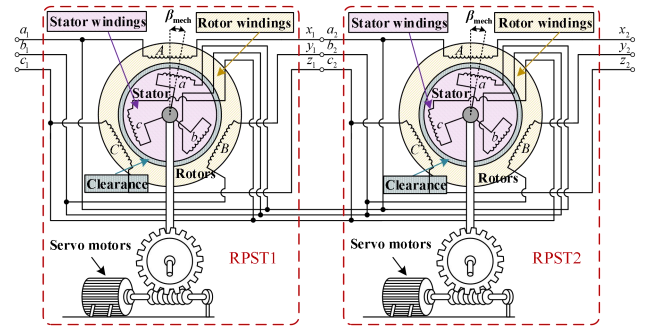


FIGURE 1 Topology structure of RPFC.

### 2.2. Working principle analysis

The single-phase equivalent circuit of RPFC is shown in Figure 2(a). In the figure,  $\dot{I}_s$  is the system line current before connection to RPFC,  $\dot{I}_{sh}$  is the total current of the rotor,  $\dot{I}_{s1}$  is the stator side current,  $\dot{U}_{RPFC}$  is the voltage of the RPFC connected in series,  $Z_{sh}$  is the impedance reduced to the rotor side,  $Z_{RPST}$  is the impedance reduced to the stator side, and  $k$  is the RPST voltage transformation ratio.

Disregarding transformer excitation current, the following relationships can be obtained in accordance with the traditional transformer analysis method:

$$\dot{U}_{rotor} = \dot{U}_s - \dot{I}_{sh} Z_{sh}, \quad (1)$$

$$\dot{U}_{RPFC} = \dot{U}_{stator1} + \dot{U}_{stator2} + 2\dot{I}_{s1} \dot{Z}_{RPST}, \quad (2)$$

$$\dot{I}_s = \dot{I}_{s1} + \dot{I}_{sh}. \quad (3)$$

From Figure 2(a), the stator and rotor voltages of the two RPSTs satisfy the following relationship:

$$\begin{cases} \dot{U}_{stator1} = \dot{U}_{rotor} k \angle \alpha_1 = (\dot{U}_s - \dot{I}_{sh} Z_{sh}) k e^{j\alpha_1} \\ \dot{U}_{stator2} = \dot{U}_{rotor} k \angle \alpha_2 = (\dot{U}_s - \dot{I}_{sh} Z_{sh}) k e^{j\alpha_2} \end{cases} \quad (4)$$

Let  $\delta = (\alpha_1 - \alpha_2)/2$  and  $\varphi = (\alpha_1 + \alpha_2)/2$ . In accordance

with Equations (2) and (4), we can obtain

$$\dot{U}_{\text{RPFC}} = (\dot{U}_s - \dot{I}_{\text{sh}} Z_{\text{sh}}) k e^{j\varphi} \cos \delta + 2 \dot{I}_{\text{s1}} Z_{\text{RPST}}. \quad (5)$$

In accordance with electromagnetic induction theorem, assuming an ideal RPST, the active and reactive power emitted or absorbed by the parallel side of RPST are equal to the active and reactive power absorbed or emitted by the series side. Therefore,

$$\dot{U}_{\text{Rotor}} \cdot \dot{I}_{\text{sh}}^* = \dot{U}_{\text{Stator}} \cdot \dot{I}_{\text{s1}}^*. \quad (6)$$

From Equations (3), (4), and (6), total rotor current and system line current can be calculated as

$$\begin{cases} \dot{I}_{\text{s1}} = \frac{\dot{I}_s}{1 + k e^{j\varphi} \cos \delta} \\ \dot{I}_{\text{sh}} = \frac{\dot{I}_s k e^{j\varphi} \cos \delta}{1 + k e^{j\varphi} \cos \delta} \end{cases} \quad (7)$$

From Equations (5) and (7), the injection voltage generated by RPFC can be calculated as

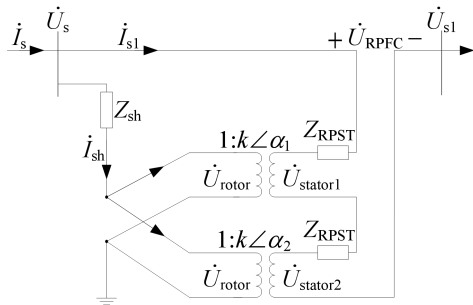
$$\dot{U}_{\text{RPFC}} = \dot{U}'_{\text{RPFC}} + \dot{I}_s Z_{\text{RPFC}}, \quad (8)$$

where

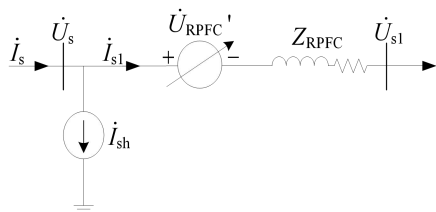
$$\dot{U}'_{\text{RPFC}} = \dot{U}_s k e^{j\varphi} \cos \delta, \quad (9)$$

$$Z_{\text{RPFC}} = \frac{2Z_{\text{RPST}} - k^2 e^{j\varphi} Z_{\text{sh}} \cos^2 \delta}{1 + k e^{j\varphi} \cos \delta}. \quad (10)$$

Thus, the simplified circuit model of RPFC can be obtained as shown in Figure 2(b). The series part consists of a controlled ideal voltage source and equivalent internal impedance. The parallel branch is a controlled current source. By changing the magnitude of  $\alpha_1$  and  $\alpha_2$ , the continuous regulation of the injected line voltage is accomplished.



(a)



(b)

FIGURE 2 Working principle of RPFC

(a) Single-phase equivalent circuit diagram of RPFC. (b) Simplified circuit model of RPFC.

### 2.3. Construction of RPFC power decoupling control model

As illustrated in Figure 3, for a typical “petal” distribution network structure,  $R_1 + jX_1$  and  $R_2 + jX_2$  respectively denote bus1 and bus2 line impedance,  $P_1 + jQ_1$  and  $P_2 + jQ_2$  represent the two lines for transmitting power,  $\dot{U}_1$  and  $\dot{U}_2$  indicate voltage on both sides of the  $K_1$  switch, and  $i$  denotes the closed-loop operation of line current.

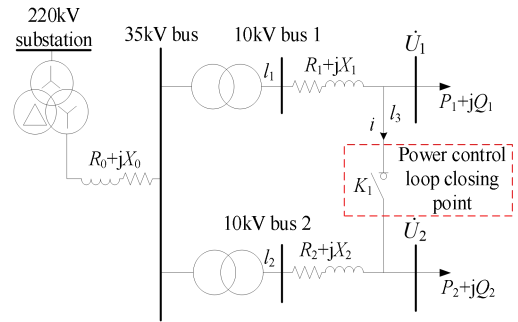


FIGURE 3 Typical “petal” distribution network structure.

RPFC is not put into operation. Lines l1 and l2 are powered in accordance with line impedance natural distribution, such that  $\dot{U}_1 = U_1 \angle 0^\circ$  and  $\dot{U}_2 = U_2 \angle \theta_g^\circ$ . By disregarding the premise of l3 resistance, the combined loop point flow through the power meet the following relationship:

$$\begin{cases} P_3 = -\frac{U_1 U_2}{X} \sin \theta_g \\ Q_3 = \frac{U_1^2}{X} - \frac{U_1 U_2}{X} \cos \theta_g \end{cases} \quad (11)$$

After RPFC is put into operation, active and reactive power between the lines are reasonably distributed by adjusting the amplitude and phase angle of string-in line voltage, limiting system power to the set range. The analysis of the power decoupling control model for accessing RPFC is as follows:

$$\dot{U}_1 = \dot{U}_2 + \dot{U}'_{\text{RPFC}} + Ri + L \frac{di}{dt}, \quad (12)$$

where  $R$  and  $L$  are the equivalent resistance and inductance of  $Z_{\text{RPFC}}$ . Let  $\dot{U}_1$  be fixed on the  $d$ -axis as the reference voltage. Then,  $\dot{U}_{1d} = \dot{U}_1$  and  $\dot{U}_{1q} = 0$ . In the steady-state case,  $di/dt = 0$  exists. At which point,

Equation (12) can be expressed in the  $dq$  coordinate system as

$$\begin{cases} U_{\text{RPFC}}'{}_d = \omega L i_q - R i_d + U_2 - U_{3d} \\ U_{\text{RPFC}}'{}_q = -\omega L i_d - R i_q - U_{3q} \end{cases} \quad (13)$$

In the  $dq$  rotating coordinate system, the transmitted power of line  $l_{1-2}$  can be expressed as

$$\begin{cases} P_{\text{ref}} = \frac{3}{2}(U_{1d}i_d + U_{1q}i_q) = \frac{3}{2}U_{1d}i_d \\ Q_{\text{ref}} = \frac{3}{2}(U_{1q}i_d - U_{1d}i_q) = -\frac{3}{2}U_{1d}i_q \end{cases} \quad (14)$$

The  $dq$ -axis component of line current  $i$  can be calculated using Equation (14).

$$\begin{cases} i_d = \frac{\sum U_d}{R^2 + \omega^2 L^2} \\ i_q = \frac{\sum U_{q1}}{R^2 + \omega^2 L^2} - \frac{\sum U_{q2}}{\omega L} \end{cases} \quad (15)$$

where  $\sum U_d$ ,  $\sum U_{q1}$ , and  $\sum U_{q2}$  are derived as shown in Appendix A, and  $\omega L \gg R$  exists in RPFC. The relationship between  $U_{\text{RPFC}}'{}_d$  and  $U_{\text{RPFC}}'{}_q$  and RPFC access point power can be calculated by substituting Equation (15) into Equation (14), as follows:

$$\begin{cases} U_{\text{RPFC}}'{}_d = U_1 - \frac{2\omega L}{3U_1} Q_{\text{ref}} - U_{2d} \\ U_{\text{RPFC}}'{}_q = -\frac{2\omega L}{3U_1} P_{\text{ref}} - U_{2q} \end{cases} \quad (16)$$

The active power of the line is only related to  $U_{\text{RPFC}}'{}_q$ , while its reactive power is only related to  $U_{\text{RPFC}}'{}_d$ . The amplitude and phase angle of RPFC output voltage can then be obtained as follows:

$$U_{\text{RPFC}}'{}_{\text{ref}} = \sqrt{U_{\text{RPFC}}'{}_d{}^2 + U_{\text{RPFC}}'{}_q{}^2}, \quad (17)$$

$$\theta_{\text{RPFC}}'{}_{\text{ref}} = \frac{180}{\pi} \arctan \frac{U_{\text{RPFC}}'{}_q}{U_{\text{RPFC}}'{}_d}. \quad (18)$$

### 3. RPFC's control strategy

#### 3.1. Variable speed control design for RPFC

The following analysis is performed in conjunction with the RPFC angle and output voltage phase diagrams, as shown in Figure 4. Through the analysis of the operating principle in Section 2.2, the values of  $\delta_{\text{ref}}$  and  $\varphi_{\text{ref}}$  can be derived from Equation (9) when  $U_{\text{RPFC}}'{}_{\text{ref}}$  and  $\theta_{\text{RPFC}}'{}_{\text{ref}}$  are known. On the basis of which, RPST rotation angle settings  $\alpha_{1\_ref}$  and  $\alpha_{2\_ref}$  are calculated.

$$\begin{cases} \alpha_{1\_ref} = \varphi_{\text{ref}} + \delta_{\text{ref}} \\ \alpha_{2\_ref} = \varphi_{\text{ref}} - \delta_{\text{ref}} \end{cases} \quad (19)$$

The actual rotation angles  $\alpha_1$  and  $\alpha_2$  of RPFC are subtracted from the settings  $\alpha_{1\_ref}$  and  $\alpha_{2\_ref}$ . Then,  $\Delta\alpha_1$  and  $\Delta\alpha_2$  are obtained through PI adjustment. The result of Equation (19) is used as the internal loop control target for the phase angle of RPFC, and  $\alpha_1$  and  $\alpha_2$  are adjusted in accordance with the set values of the two rotation angles to control output voltage amplitude and phase to meet the set requirements and achieve control of line power.

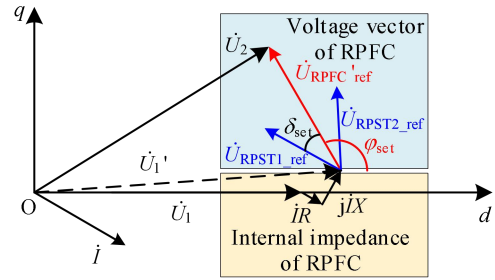


FIGURE 4 Phasor diagram of RPFC's output voltage.

The servomotor controls the two RPSTs via PWM, and the speed of the RPSTs is changed by adjusting the duty cycle. The change in output voltage when RPFC is regulated at a constant speed is illustrated in Figure 5. The deviation of the two rotation angles from the set value during operation is typically not the same. Therefore, one RPST stops rotating when the set value is reached, while the other RPST continues to operate, resulting in periodic oscillations in RPFC output power.

Let  $t=t_0$  moment.  $\dot{U}_{\text{RPST1}}$  reached the set value  $\dot{U}_{\text{RPST1\_ref}}$ , whereas  $\dot{U}_{\text{RPST2}}$  did not reach the set value  $\dot{U}_{\text{RPST2\_ref}}$ . At this moment,  $\Delta\alpha_1=0$  and  $\Delta\alpha_2 \neq 0$ . Then,  $\alpha_1$  stops rotation, and servo motor control  $\alpha_2$  continues to run in the direction of the set value.

When  $t=t_1$  moment, line power changes because the action of  $\alpha_2$  changes the output voltage of RPFC at this time. Equation (16) will calculate the new stator voltage set values  $\dot{U}_{\text{RPST1\_ref}}$  and  $\dot{U}_{\text{RPST2\_ref}}$ . Thus, the originally stopped  $\alpha_1$  will rerun, while  $\alpha_2$  will continue to rotate in the direction of the new set value, finally causing output power within the range of the set value to oscillate repeatedly.

On this basis, the two groups of servo motors are designed for coordinated speed control, such that  $\alpha_1$  and  $\alpha_2$  meet the simultaneous stopping motion within the set value. The specific design scheme is shown in Figure 6.

When the angular difference between the set and actual values of  $\Delta\alpha_1$  and  $\Delta\alpha_2$  of the two sets of rotary transfer phase transformers differs and neither is 0, the PWM wave duty cycle of the two servo motors is quantized and calculated to exist at  $\Delta\alpha_j < \Delta\alpha_i$ .

$$\begin{cases} D_i = D \\ D_j = \frac{1}{q} \times \text{round}(q \times \text{sat}(\frac{\Delta\alpha_j}{\Delta\alpha_i}))D \end{cases}, \quad (20)$$

where  $i, j \in (1, 2)$ , and  $q$  is an integer greater than 1 that is used to quantify the size of the duty cycle of a servo motor. The sat function will rotate the angle of error to be greater than the size of the limit between 0 and 1 to prevent a denominator of 0 and lead to an infinite duty cycle. The round function will be the value of the rounding operation.

When  $\Delta\alpha_2 < \Delta\alpha_1$ , as shown in Figure 6(a), the PWM wave duty cycle  $D_1 = D$ .  $\omega_1$  maintains maximum speed. The PWM wave duty cycle  $D_2$  is quantized and calculated to reduce the size of the duty cycle and lower  $\omega_2$  speed, such that  $\alpha_1$  and  $\alpha_2$  reach the set value simultaneously.

Similarly when  $\Delta\alpha_1 < \Delta\alpha_2$ , as shown in Figure 6(b), the servo motor speed  $\omega_2$  of RPST2 maintains maximum speed. The PWM wave of RPST1 is quantized and calculated to reduce the size of the duty cycle and lower  $\omega_1$  speed to achieve adaptive adjustment of speed.

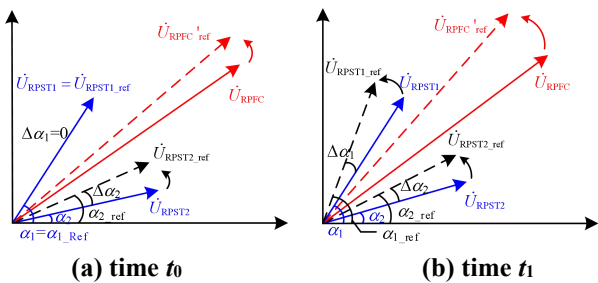


**FIGURE 5** Phasor diagram of RPFC's output voltage during constant speed regulation.

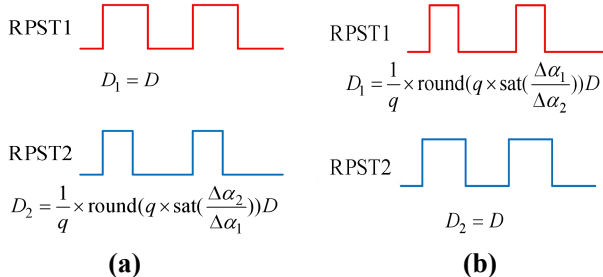


**FIGURE 6** Phase angle control during adaptive speed

regulation. (a) Case of  $\Delta\alpha_2 < \Delta\alpha_1$ . (b) Case of  $\Delta\alpha_1 < \Delta\alpha_2$ .

### 3.2. Servo motor–RPST synchronous rotation design

As shown in Figure 7(a), servo motors 1 and 2 rotate RPST1 and RPST2, respectively, through the gears. However, due to the gap between the worm and RPST gears, as shown in Figure 7(b), during the process of changing the servo motor from forward operation to reverse operation, the phenomenon of the servo motor and RPST rotation not being synchronized at this time may lead to errors between the actual and set values during power control, or even cause the two sets of RPSTs to exit the variable speed regulation state, making the output power oscillate repeatedly around the set value range.

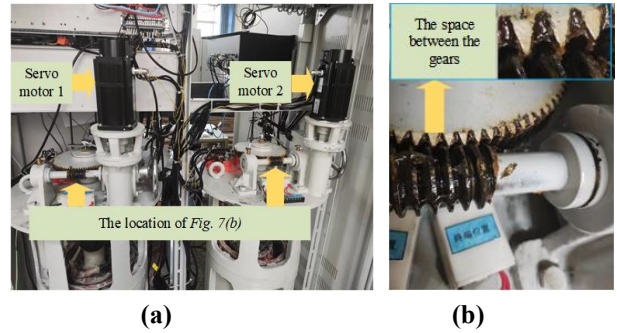


**FIGURE 7** Connection relationship between servo motors: turbine worm and RPST. (a) Servo motor–RPST association mode. (b) Gap between gear and RPST.

To address this problem, the angular differences between RPST rotor angle before and after the moment are compared. To discriminate the rotational asynchronous problem, when RPST rotational speed is slow, the control system may misjudge the system into or out of the rotational asynchronous state. Therefore, the accumulator module is added to assist in discriminating RPST running state, and its specific steps include the following.

(1) When servo motor steering changes at  $t_0$ , the servo motor maintains the rotating action but the actual RPST does not act. The system may enter the rotating asynchronous state, make  $slip = -1$ , and use  $slip\_cnt$  to accumulate slip. When  $slip\_cnt$  is less than a certain range, RPST is considered to enter the rotating asynchronous state. At this point  $inverse = 1$ .

(2) When the system is in rotating asynchronous state, the rotation process of the servo motor should be defaulted to invalid rotation and not counted in the overall

regulation control block diagram. At this time,  $\alpha_{ref}=\alpha_{i0}$ .

(3) When RPST rotation angle  $\alpha$  changes, the system may be out of the rotation asynchronous state. At this time, make  $slip=1$ , and use  $slip\_cnt$  to accumulate slip. When  $slip\_cnt$  is greater than a certain range, think RPST end rotation asynchronous. At this time,  $\alpha_{ref}=\alpha_{ref}$ .

### 3.3. Variable domain fuzzy PI controller design

Influenced by frequent changes in line load parameters, the control effect achieved by the fixed  $K_p$  and  $K_I$  coefficients performs poorly; hence, the PI controller is proposed to be improved by means of a fuzzy controller to achieve the dynamic regulation of the  $K_p$  and  $K_I$  coefficients. However, the complexity exhibited by dual power supply systems and access to a high proportion of renewable energy make meeting the regulation requirements in a fixed theoretical domain difficult for the fuzzy controller. To address this problem, the literature [22] proposed a variable-domain fuzzy PI control method that consists of a base fuzzy controller with a scaling factor that regulates its theoretical domain.

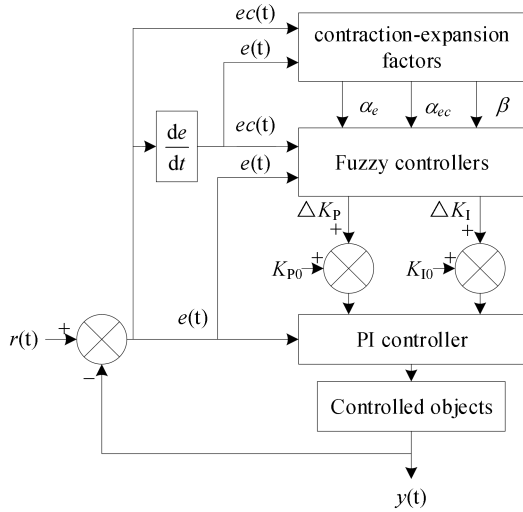


**FIGURE 8** Structure diagram of the variable-domain fuzzy PI controller.

As shown in Figure 8, the expression for the transfer function of the PI controller at this point is as follows:

$$y(t) = (K_{p0} + \Delta K_p)e(t) + (K_{I0} + \Delta K_I) \cdot \int_0^t e(t) dt . \quad (21)$$

In the fuzzy PI controller,  $e(t)$  and  $ec(t)$  are taken as the input variables  $x_i(t)$  of the fuzzy controller, where  $x_1(t)=e(t)$  and  $x_2(t)=ec(t)$ ;  $\Delta K_p(t)$  and  $\Delta K_I(t)$  are taken as the output variables  $y_j(t)$  of the fuzzy controller, where

$y_1(t)=\Delta K_p(t)$  and  $y_2(t)=\Delta K_I(t)$ ; and its initial domain is determined by the input. The maximum range of variation of the output variables determines their initial theoretical domain, where  $x_i(t)=[-E_i, E_i]$  and  $y_j(t)=[-U_j, U_j]$ .  $E_i$  and  $U_j$  are the domain boundaries.

The exact values on the theoretical domain are then converted into the corresponding fuzzy subsets, which are divided into seven fuzzy sets: NB (negative large), NM (negative medium), NS (negative small), ZE (zero), PS (positive small), PM (positive medium), and PB (positive large). From the literature [23] and combined with the experimental analysis results, the fuzzy rules of  $\Delta K_p$  and  $\Delta K_I$  are derived as shown in Exhibits **B1** and **B2**, respectively.

Variable-domain fuzzy control achieves dynamic changes in the input and output domains through a scaling factor. Consequently, the input domain  $[-E_i, E_i]$  and output domain  $[-U_j, U_j]$  are adaptively adjusted as the input signals  $e(t)$  and  $ec(t)$  change and when  $x_i(t)$  and  $y_j(t)$  exist.

$$x_i(t) = [-\alpha_i(t) \cdot E_i, \alpha_i(t) \cdot E_i] , \quad (22)$$

$$y_j(t) = [-\beta_j(t) \cdot U_j, \beta_j(t) \cdot U_j] , \quad (23)$$

where  $\alpha_i$  and  $\beta_j$  are the scaling factors of the input and output theoretical domains, respectively. In the case of constant control rules, the shrinkage of the theoretical domain is equivalent to an increase in the control rules, i.e., the distance between the peak points of the fuzzy set shrinks and interpolation accuracy increases, as shown in Figure 9 for the basic principle of variable theoretical domain fuzzy control.

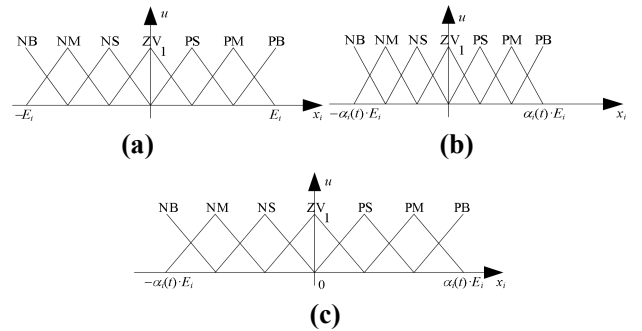


**FIGURE 9** Basic principles of variable domain. (a) Initial domain of the argument. (b) Systolic state theory domain. (c) Expanding the state of the domain.

The traditional function-based stretching factor requires the construction of a function and the setting of

parameters. An improper selection of function form or setting of parameters can exert a considerable influence on the effect of the domain, and thus, it is less versatile. Meanwhile, the stretching factor designed based on fuzzy reasoning describes the domain adjustment law through linguistic concepts without the need to construct an accurate function model. Thus, it exhibits certain versatility and high practical value.

For the input domain stretching factor, when the error  $e(t)$  and its rate of change  $ec(t)$  are large, a larger stretching factor is outputted to expand the domain and accelerate convergence. When the error  $e(t)$  and its rate of change are small, a smaller stretching factor is outputted to reduce the domain, encrypt the fuzzy division, increase the available control rules, and improve the control accuracy and stability, as indicated in Appendix B3.

For the output domain stretching factor, the

stretching factors  $\beta_P$  and  $\beta_I$  should be developed for the output domains  $\Delta K_P$  and  $\Delta K_I$ , respectively, on the basis of the power regulation output characteristics. Combined the literature [24] and the results of the experimental analysis, the linguistic values of  $\beta_P$  and  $\beta_I$  are expressed in terms of {very small, small, medium, large, very large}, corresponding to the fuzzy combination {VS, S, M, B, VB}. The output variables have a domain of [0,1]. In particular, fuzzy rules are shown in Appendices B4 and B5.

### 3.4. Control block diagram of RPFC

To improve the control effect of RPFC in the power control scenario, RPFC variable speed control is added to the phase angle link, and variable domain fuzzy PI control is added to the power link. Meanwhile, a servo motor–RPST synchronous rotation scheme is designed to improve RPFC stability and regulation accuracy for the shortcomings of the RPFC mechanical structure.

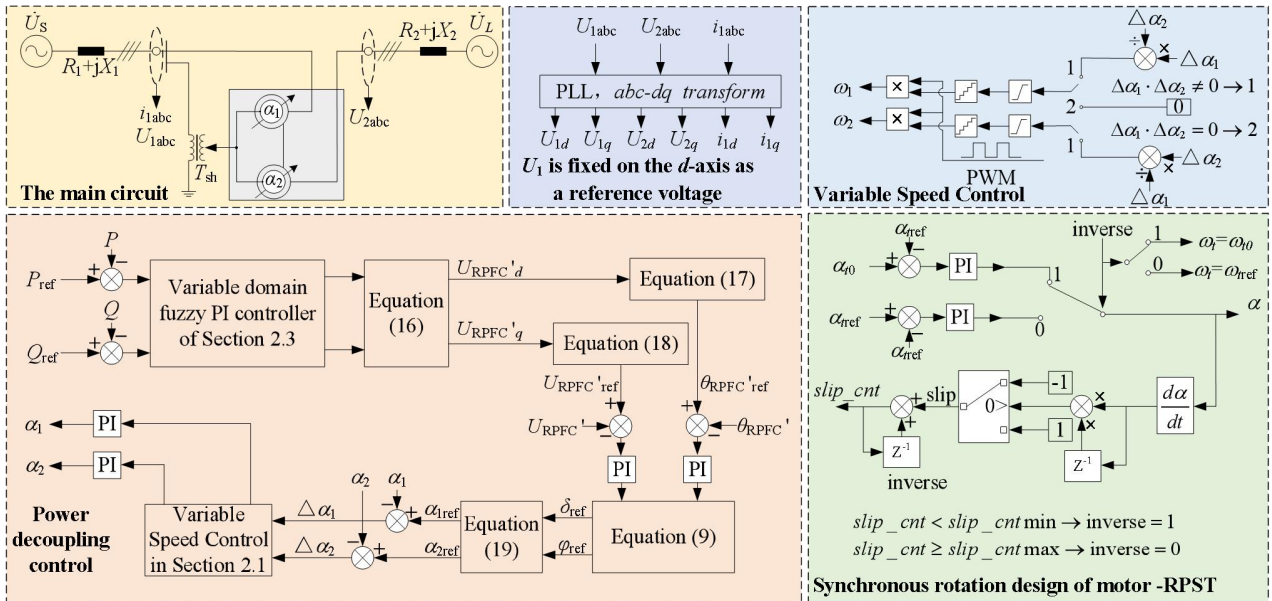


FIGURE 10 Power decoupling control strategy of RPFC.

## 4. Experimental verification

### 4.1. Construction of experimental platform

To verify the validity and correctness of the RPFC power decoupling model and control strategy proposed in this study, a 380 V/40 kVA experimental prototype (Figure 11) was developed in a laboratory. The experimental scenario in Figure 12 was built to verify the RPFC power control function. The primary part of RPFC in the experimental platform consisted

of two sets of rotary transfer phase transformers with a variable ratio of 380:100 and a capacity of 20 kVA. The control module used a digital signal processor (DSP) controller. The controller voltage was provided by a programmable logic controller AC 220 V to DC 24 V power supply. Servo motor speed was normalized to RPST rotor speed of 1°/s. The parameters of RPFC and experimental system are provided in Appendix B6.

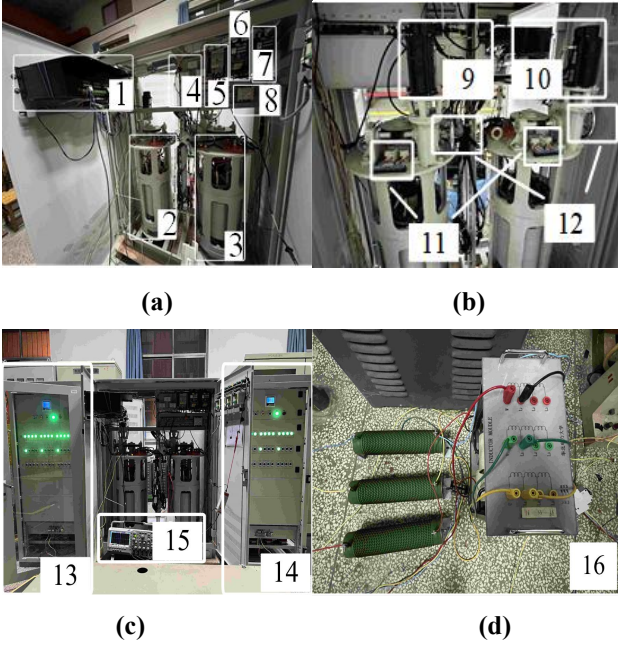


**FIGURE 11** Experimental platform of RPFC. (a) Internal structure of RPFC. (b) Structure of the servo motor drive module. (c) Experimental load. (d) Resistance and inductance.

In Figure 11(a), 1 is a DSP processor, 2 and 3 are two RPSTs, 4 is a current collector, 5 is an RPST energy-taking side input switch that closes automatically when power supply generates excitation to the rotor winding and opens automatically when excitation is removed, 6 is a series closure switch, 7 is a parallel bypass switch, and 8 is an RS485 interface. Figure 11(b) provides further illustration of Figures 7, 9, and 10. It shows two sets of servo motors that correspond to RPST. 11 is a manually controlled worm gear, and 12 is a position relay. In Figure 11(c), 13 and 14 are load boxes, and 15 is an oscilloscope. In Figure 11(d), 16 is a resistive and inductive element.

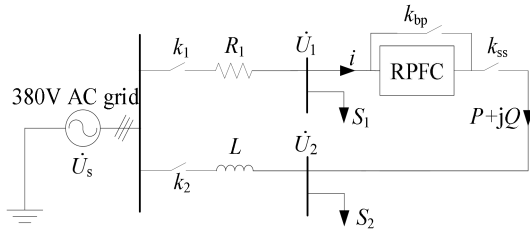


**FIGURE 12** Power control of dual power supply based on RPFC.

## 4.2. Experiments in precise power regulation

### 4.2.1 Regulation of variable power setting values

A variable power set point experiment was

performed in accordance with Figure 12. The experiment was divided into five stages by varying the line power set point  $P_{\text{ref}}+jQ_{\text{ref}}$ .

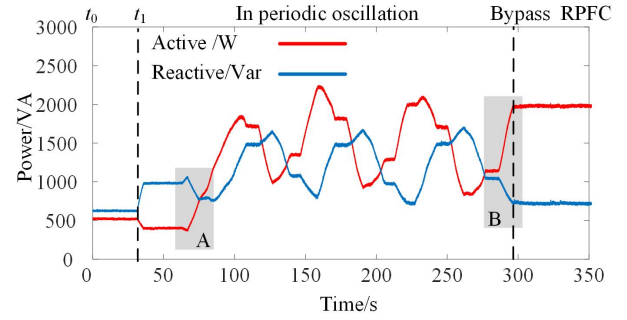
Stage 1  $t_0-t_1$ :  $P_{\text{ref}}+jQ_{\text{ref}}=500+j500$  VA.

Stage 2  $t_1-t_2$ :  $P_{\text{ref}}+jQ_{\text{ref}}=1000+j500$  VA.

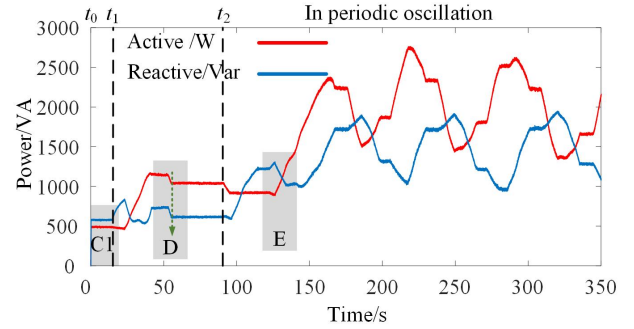
Stage 3  $t_2-t_3$ :  $P_{\text{ref}}+jQ_{\text{ref}}=1000+j1000$  VA.

Stage 4  $t_3-t_4$ :  $P_{\text{ref}}+jQ_{\text{ref}}=2000+j1000$  VA.

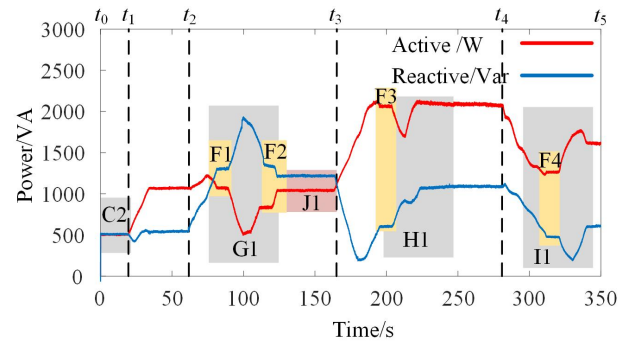
Stage 5  $t_4-t_5$ :  $P_{\text{ref}}+jQ_{\text{ref}}=1500+j500$  VA.



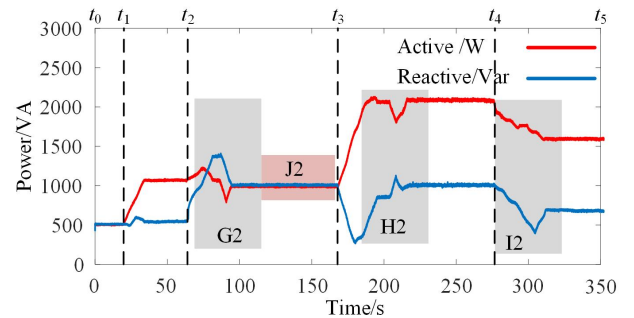
(a)



(b)



(c)



(d)

**FIGURE 13** Experiment of variable power set point based on RPFC. (a) Experimental results of the uniform speed control scheme. (b) Experimental results of the variable speed control scheme. (c) Experimental results of the synchronous rotation control of the servo motor and RPST. (d) Experimental results of the improved RPFC control strategy proposed in this study.

RPFC that uses uniform speed control when line power controls the experimental waveform is shown in Figure 13(a), corresponding to the RPFC phase angle loop and voltage loop dynamic control process, as shown in Appendix C1. In the regulation process of Stage 2, one RPST reaches the set angle and another RPST is still not running at the end of the situation, resulting in the phenomenon of periodic oscillation of line power, followed by the closure of the bypass switch kbp to avoid device failure.

When the RPFC joined the control scheme of variable speed, but had not yet been designed for the synchronous rotation scheme, the experimental waveform is shown in Figure 13(b), corresponding to the RPFC phase angle loop and voltage loop dynamic control process, as shown in Appendix C2. By position D of the variable speed control, the line active power and reactive power take the same moment to complete the regulation. By position C1, ? can be seen due to RPFC's mechanical structure caused by the gear gap, which seriously affects power control accuracy. It may have an effect on variable speed control under specific power regulation conditions, causing system periodic oscillation problem at position E.

As shown from position C2 in Figure 13(c) of the experimental waveform, the addition of RPST–servo motor synchronous rotation effectively improves system control accuracy compared with position C1. An effective and accurate power control can be accomplished during all stages of regulation. However, at positions G1, H1, and I1, a greater degree of overshoot can be observed when the conventional PI closed-loop controller is used. From position J1, its control accuracy can still be improved, corresponding to the RPFC phase angle loop and voltage loop

dynamic control process, as shown in Appendix C3.

With the improved RPFC control strategy proposed in this study, positions G2, H2, I2, and J2 in Figure 13(d) show that RPFC can quickly and accurately adjust line transmission power to respond to the power control needs of the distribution network when the set value changes, corresponding to the RPFC phase angle loop and voltage loop dynamic control process, as shown in Appendix C4.

#### 4.2.2 Regulation of variable loads with constant transmitted power

A variable load–constant transmission power experiment was performed in accordance with Figure 12, at which point the line power was set to  $P_{ref}+jQ_{ref}=2+j1.5$  kVA. The experiment was divided into four phases.

Stage 1  $t_0-t_1$ :  $S_1=3300+j1200$  VA,  $S_2=2400+j500$  VA.

Stage 2  $t_1-t_2$ :  $S_1=3300+j1200$  VA,  $S_2=1200+j500$  VA.

Stage 3  $t_2-t_3$ :  $S_1=2400+j800$  VA,  $S_2=1200+j500$  VA.

Stage 4  $t_3-t_4$ :  $S_1=1200+j300$  VA,  $S_2=1200+j500$  VA.

From positions A1, A2, and A3 in Figure 14, we can observe that the use of a variable speed control scheme can effectively ensure the stability of RPFC power control. Positions B1, B2, and B3 in the figure show the servo motor–RPST synchronous rotation control process. From the experimental results, good control effect can be seen under variable load–constant transmission power experimental conditions.

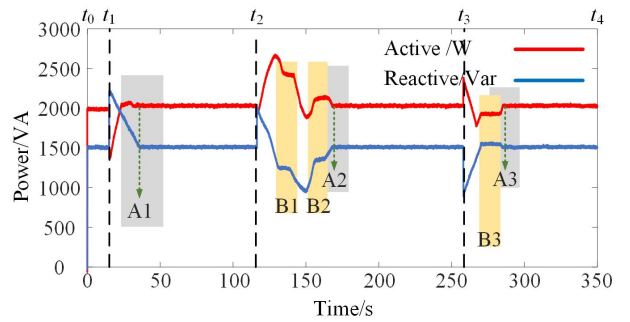


**FIGURE 14** Variable load–constant transmission power based on RPFC

---

## 5. Conclusion

To achieve the safe operation of a “petal”-type active distribution network, a solution is proposed to connect RPFC at the loop closure point to achieve accurate control of the power of the looped line. Through theoretical analysis and experimental verification, the following conclusions are obtained.

1) The proposed RPFC control system consists of a power inner loop, a voltage loop, and a phase angle outer loop. By changing the relative angle of the two RPST stator rotors, continuous regulation of the injected voltage can be completed, achieving flexible control of line power. The electromagnetic structure ensures that RPFC can still exhibit stable control effects in case of system faults.

2) The variable-domain fuzzy PI controller introduced into the RPFC power inner-loop control link can effectively improve the disadvantages of poor robustness of cross-decoupling control applicable to power control in distribution networks. It significantly improves system dynamic power control effect.

3) In the RPFC phase angle outer loop control link, the output duty cycle size is dynamically adjusted by quantization calculation of the PWM wave, solving the problem of double RPST periodic oscillation. The servo motor–RPST synchronous rotation control scheme is designed to address the disadvantage of the RPFC’s mechanical structure, effectively reducing static system power error.

## 6. References

1. H. Liangliang and L. Siyu.:Automatic Switchover System Scheme for 20kV Petal-shape Distribution Network Non-communication Protection. In:2019 IEEE 8th International Conference on Advanced Power System Automation and Protection (APAP), 30(2), 552-555(2019).
2. J. Kong, Y. Li, W. Yao. et al. :Backup Protection for Tie Lines in a Double-Petal-mode Distribution Network. In:2021 IEEE International Conference on Electrical Engineering and Mechatronics Technology (ICEEMT), 212-215(2021).
3. B. Chen, W. Fei, C. Tian et al. :Research on an Improved Hybrid Unified Power Flow Controller. In:IEEE Transactions on Industry Applications, 54(6), 5649-5660(2018).
4. X. Zhong, M. Zhu, Y. Chi, et al. :Composite DC Power Flow Controller. In:IEEE Transactions on Power Electronics, 35(4), 3530-3542(2020).
5. J. Lin, B. Zhang, L. Gao. et al. :Multi-mode Coordination System Control Strategy and Its Operation Performance of Western Nanjing Power Grid UPFC Project. In:2018 International Conference on Power System Technology (POWERCON), 2678-2684(2018).
6. M. Hosseini Abardeh and R. Ghazi. Rotary power flow controller (RPFC) characteristics analysis. In:2011 5th International Power Engineering and Optimization Conference, 358-363(2011).
7. D. R. Ivic and P. C. Stefanov.: An Extended Control Strategy for Weakly Meshed Distribution Networks With Soft Open Points and Distributed Generation. In:IEEE Access, 9, 37886-137901(2021).
8. S. D. Choudante and A. A. Bhole. et al. :A Review: Voltage Stability and Power Flow Improvement by Using UPFC Controller. In:2018 International Conference on Computation of Power, Energy, Information and Communication (ICCPEIC), 462-465(2018).
9. S. Chansareewittaya. :Enhancing ratio of TTC per fuel cost using evolutionary programming with UPFC. In:2018 5th International Conference on Business and Industrial Research (ICBIR), 303-308(2018).
10. A. O. Ba, T. Peng and S. Lefebvre. :Rotary Power-Flow Controller for Dynamic Performance Evaluation—Part I: RPFC Modeling. In:IEEE Transactions on Power Delivery, 24(3),1406-1416, (2009).
11. Zhenlong Tan, Chunpeng Zhang and Qirong Jiang.:Research on characteristics and power flow control strategy of rotary power flow controller. In:2015 5th International Youth Conference on Energy (IYCE), 1-8(2015).
12. S. Thakare, M. Janaki and R. Thirumalaivasan. :Improvement in Power Flow Control and Voltage Regulation using UPFC. In2019 Innovations in Power and Advanced Computing

---

Technologies (i-PACT), 1-4(2019).

13. Y. Zhang, H. F. Li, w. J. Du. et al.:Coordinated damping control of phase angle controlled and vector controlled UPFC — A comparative study.In 12th IET International Conference on AC and DC Power Transmission (ACDC 2016), 1-6(2016).

14. P. Jagtap and V. Chandrakar. :Comparative Study of UPFC Controllers to Improve Transient and Dynamic Stability of Power System. In:2021 IEEE 4th International Conference on Computing, Power and Communication Technologies (GUCON), 1-7(2021).

15. A. O. Ba, T. Peng and S. Lefebvre. :Rotary Power-Flow Controller for Dynamic Performance Evaluation—Part II: RPFC Application in a Transmission Corridor. In:IEEE Transactions on Power Delivery, 24(3),1417-1425(2009).

16. S. Yang, Y. Liu, X. Wang, D. Gunasekaran, U. Karki and F. Z. Peng, "Modulation and Control of Transformerless UPFC," in IEEE Transactions on Power Electronics, 31(2) pp. 1050-1063(2016).

17. F. M. Albatsh, S. Ahmad, S. Mekhilef. et al.:D - Q model of fuzzy based UPFC to control power flow in transmission network. In:7th IET International Conference on Power Electronics, Machines and Drives, 1-6(2014).

18. I. G. Odnokopylov, Y. N. Dementev, I. V. Usachev. et al.:Load balancing of two-motor asynchronous electric drive. In:2015 International Siberian Conference on Control and Communications (SIBCON).

19. L. Zhao, X. Zhang and J. Ji. :A torque control strategy of brushless direct current motor with current observer. In:2015 IEEE International Conference on Mechatronics and Automation (ICMA), 303-307 (2015).

20. Y. Zheng, H. Qu, Y. Zhao. et al.:Synchronous Control of Multi-Motor Systems Using an Improved Relative Coupling Control Structure. In:2022 IEEE 11th Data Driven Control and Learning Systems

Conference (DDCLS), 1427-1432(2022).

21. P. Gao, G. Zhang, H. Ouyang. et al.:An Adaptive Super Twisting Nonlinear Fractional Order PID Sliding Mode Control of Permanent Magnet Synchronous Motor Speed Regulation System Based on Extended State Observer. In:IEEE Access, 8, 53498-53510(2020).

22. H. Li, H. Xu, R. Jiang. et al.:Research on Variable Universe Fuzzy Control of Double-Loop Mode Buck-Boost Converter Based on Matlab. In2021 IEEE 4th International Conference on Information Systems and Computer Aided Education (ICISCAE), 17-21(2021).

23. C. Chen, C. Chang and X. Han. :Design of Equivalent Single-Input Fuzzy PI Converter for Buck DC-DC Converters with Excellent Transient Performance. In2019 IEEE 3rd International Electrical and Energy Conference (CIEEC), 335-340 (2019),.

24. X. Zhang, F. Li and K. Ding. :Study on Droop Frequency Modulation of Micro-Grid Based on Variable Domain Fuzzy PI. In:2019 IEEE 3rd Conference on Energy Internet and Energy System Integration (EI2), 1976-1979(2019).

## Appendix A

$$\begin{cases} 0 = \omega L i_q - R i_d + U_{1d} - U_{2d} - U_{RPFC}'_d \\ 0 = -\omega L i_d - R i_q + U_{1q} - U_{2q} - U_{RPFC}'_q \end{cases} \quad (A1)$$

So there are:

$$\begin{cases} Ri_d - \omega Li_q = U_{1d} - U_{2d} - U_{\text{RPFC}'_d} \\ \omega Li_d + Ri_q = U_{1q} - U_{2q} - U_{\text{RPFC}'_q} \end{cases} \quad (\text{A2})$$

$$\begin{cases} \frac{R^2}{\omega L} i_d - Ri_q = \frac{R}{\omega L} U_{1d} - \frac{R}{\omega L} U_{2d} - \frac{R}{\omega L} U_{\text{RPFC}'_d} \\ \omega Li_d + Ri_q = U_{1q} - U_{2q} - U_{\text{RPFC}'_q} \end{cases} \quad (\text{A3})$$

We can get

$$i_d = \frac{1}{R^2 + \omega^2 L^2} (RU_{1d} - RU_{2d} - RU_{\text{RPFC}'_d} - \omega LU_{2q} - \omega LU_{\text{RPFC}'_q}) \quad (\text{A4})$$

$$i_q = \frac{1}{R^2 + \omega^2 L^2} \left( \frac{R^2}{\omega L} U_{1d} - \frac{R^2}{\omega L} U_{2d} - \frac{R^2}{\omega L} U_{\text{RPFC}'_d} - RU_{2q} - RU_{\text{RPFC}'_q} \right) - \frac{1}{\omega L} U_{1d} + \frac{1}{\omega L} U_{2d} + \frac{1}{\omega L} U_{\text{RPFC}'_d} \quad (\text{A5})$$

The values of  $\sum U_d$ ,  $\sum U_{q1}$  and  $\sum U_{q2}$  can be obtained as:

$$\sum U_d = RU_{1d} - RU_{2d} - RU_{\text{RPFC}'_d} - \omega LU_{2q} - \omega LU_{\text{RPFC}'_q} \quad (\text{A6})$$

$$\sum U_{q1} = \frac{R^2}{\omega L} U_{1d} - \frac{R^2}{\omega L} U_{2d} - \frac{R^2}{\omega L} U_{\text{RPFC}'_d} - RU_{2q} - RU_{\text{RPFC}'_q} \quad (\text{A7})$$

$$\sum U_{q2} = U_{1d} + U_{2d} + U_{\text{RPFC}'_d} \quad (\text{A8})$$

## Appendix B

**TABLE B1** Fuzzy rule for  $\Delta K_P(t)$

$\Delta K_P(t)$	$ec(t)$						
	NB	NM	NS	ZE	PS	PM	PB
NB	PB	PB	PM	PM	PS	ZE	ZE
NM	PB	PM	PM	PS	PS	ZE	ZE
NS	PM	PM	PM	PS	ZE	NS	NS
$e(t)$	ZE	PM	PS	PS	ZE	NS	NM
	PS	PS	PS	ZE	NS	NS	NM
	PM	ZE	ZE	NS	NM	NM	NB
	PB	ZE	NS	NS	NM	NB	NB

**TABLE B2** Fuzzy rule for  $\Delta K_I(t)$

$\Delta K_I(t)$	$ec(t)$						
	NB	NM	NS	ZE	PS	PM	PB
NB	NB	NB	NM	PM	NS	NS	ZE
NM	NB	NM	NM	PS	NS	ZE	ZE
NS	NB	NM	NS	PS	ZE	PS	PS
$e(t)$	ZE	NM	NS	NS	ZE	PS	PM
	PS	NM	NS	ZE	NS	PS	PM
	PM	NS	ZE	PS	NM	PM	PB
	PB	ZE	ZE	PS	NM	PM	PB

**TABLE B3** Enter the fuzzy rule for the scaling factor  $\alpha_i$

$\alpha_i$	$ec(t)$						
	NB	NM	NS	ZE	PS	PM	PB
$e(t)$	NB	PB	PB	PM	PM	PM	PB

NM	PB	PM	PS	PS	PS	PM	PB
NS	PM	PS	PS	PZ	PS	PS	PM
ZE	PS	PS	PZ	PZ	PZ	PS	PS
PS	PM	PS	PS	PS	PS	PS	PM
PM	PB	PM	PS	PS	PS	PM	PB
PB	PB	PB	PM	PM	PM	PB	PB

**TABLE B4** Fuzzy rules for outputting the scaling factor

$\alpha_i$	$\beta_P$						
	$ec(t)$						
	NB	NM	NS	ZE	PS	PM	PB
$e(t)$	NB	VB	VB	VB	B	B	M
	NM	VB	VB	B	B	B	M
	NS	VB	B	B	B	M	S
	ZE	B	B	B	M	S	S
	PS	B	B	M	S	S	VS
	PM	M	M	S	S	S	VS
	PB	M	S	S	S	VS	VS

**TABLE B5** Fuzzy rules for outputting the scaling factor

$\alpha_i$	$\beta_I$						
	$ec(t)$						
	NB	NM	NS	ZE	PS	PM	PB
$e(t)$	NB	VS	VS	VS	S	S	M
	NM	VS	VS	VS	S	S	M
	NS	VS	S	S	S	M	B

ZE	S	S	S	M	B	B	B
PS	S	S	M	B	B	B	VB
PM	M	M	B	B	B	VB	VB
PB	M	M	B	B	VB	VB	VB

**TABLE B6** 40KVA-RPFC system parameters

Parameter	Values
DRPST capacity /kVA	40
Frequency /Hz	50
Input voltage /V	380
Output voltage /V	100
Servo motor rated speed r/min	600
Load power $S_1$ /VA	3300+j1200
Load power $S_2$ /VA	2400+j500
Series resistance $L/\Omega$	0+j5
Series reactance $R/\Omega$	5+j0

### Appendix C

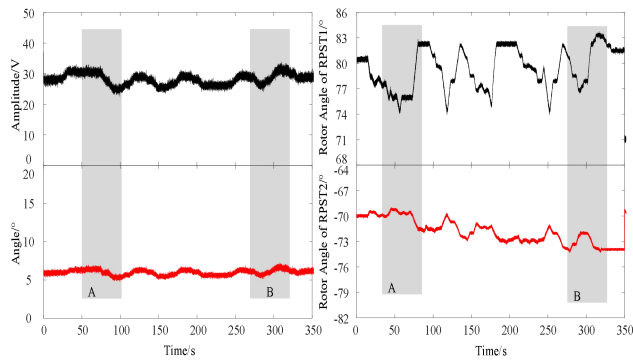


**FIGURE C1** Control process of servo motor -RPST constant speed

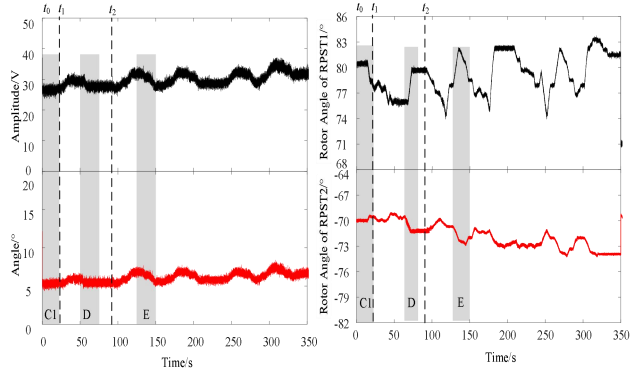


**FIGURE C2** Variable speed control process of RPFC

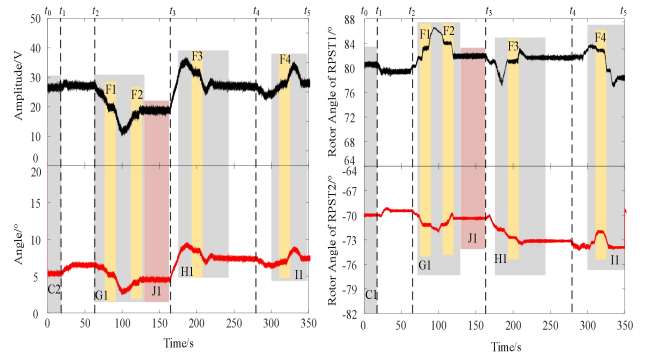


**FIGURE C3** Control process of servo motor and RPST co-rotation

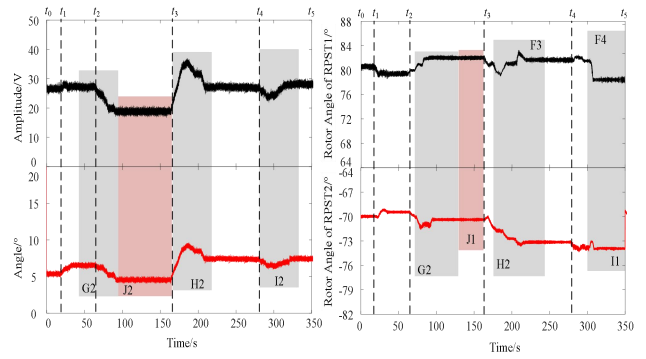


**FIGURE C4** Control process of the improved RPFC control strategy proposed in this study